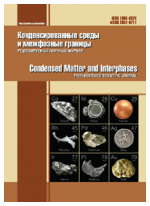

ISSN 1606-867X (Print)
ISSN 2687-0711 (Online)
Condensed Matter and Interphases
Kondensirovannye Sredy i Mezhfaznye Granitsy
https://journals.vsu.ru/kcmf/

Original articles

Research article
https://doi.org/10.17308/kcmf.2023.25/10646

Synthesising dispersed powders of CoZn ferrites for microwave absorption

D. V. Ivashenko[1]✉, D. A. Urbanovich[1], I. Y. Polyn[1], M. V. Bushinsky[2], A. V. Trukhanov[2], V. V. Pankov[1]

[1]*Belarusian State University,*
4 Nezavisimosti avenue, Minsk 220030, Belarus

[2]*SSPA "Scientific-Practical Materials Research Centre of NAS of Belarus"*
19 Pietrusia Broŭki, Minsk 220072, Belarus

Abstract

An important task of chemical materials science is to obtain materials with set parameters and to provide a reliable prediction of their properties. At the moment, an important task is to develop promising absorbing coatings based on dispersed magnetic materials. To ensure more effective use of dispersed powders of cobalt-zinc ferrite for fillers absorbing microwave radiation, we studied the changes in their magnetic properties and morphology depending on the conditions of the sol-gel synthesis.

In our study, we synthesised $Co_{0.65}Zn_{0.35}Fe_2O_4$ ferrite powders of various degree of dispersion using the sol-gel method. The samples were analysed using X-ray diffractometry. The microstructure and the morphology of the nanoparticles were studied by means of scanning electron microscopy. The ratio of the concentration of metal atoms in ferrite powders and the features of their distribution on the surface of the particles were determined by energy dispersive X-ray spectroscopy. Magnetometry was used to determine the specific saturation magnetization and the coercive force.

The study demonstrated that the main factor resulting in low values of the saturation magnetization of the cobalt ferrite nanopaticles is the formation of the magnetic dead layer on their surface. This layer is formed due to a number of factors including noncollinearity of spins, disordering of cations, defectiveness, amorphous state, and the difference in the composition occurring because the processes of reciprocal diffusion of cations during and the formation of the spinel structure during the synthesis are not complete.

The study determined the ways to reduce the size of the inactive magnetic layer by controlling the parameters of the sol-gel synthesis in order to find effective methods of obtaining ferrite powders with increased magnetization, degree of crystallinity and the intermediate particles size between a superparamagnetic and a multidomain state. Such materials can be used as fillers for coating absorbing microwave radiation.

Keywords: Cobalt-zinc ferrite, Microwave absorption, Sol-gel synthesis, Nanoparticles

For citation: Ivashenko D. V., Urbanovich D. A., Palyn I. U., Bushinsky M. V., Trukhanov A. V., Pankov V. V. Synthesising dispersed powders of CoZn ferrites for microwave absorption**.** *Condensed Matter and Interphases*. 2023;25(1): 37–46. https://doi.org/10.17308/kcmf.2023.25/10646

***Для цитирования*:** Ивашенко Д. В., Урбанович Д. А., Полын И. Ю., Бушинский М. В., Труханов А.В., Паньков В. В. Процессы синтеза дисперсных порошков CoZn ферритов для микроволнового поглощения. *Конденсированные среды и межфазные границы*. 2023;25(1): 37–46. https://doi.org/10.17308/kcmf.2023.25/10646

✉ Ivashenko D. V., e-mail: ivashenkodm@gmail.com

1. Introduction

Ferrites are used in a large number of industries, but they are also actively used as microwave absorption materials. Recently, manufacturers have also focused on nanosized powders, which are used in biomedical diagnostics and medicine [1, 2]. However, we should point out that the use of highly dispersed magnetic particles as, for instance, absorbers of electromagnetic radiation or electronic components for creating magnetic fields can be rather difficult. The problem lies in the fact that, when using such particles, the saturation magnetization of nanosized magnetic materials is often lower than that of bulk samples [3, 4]. A decrease in the saturation magnetization of ferrites following the transition to the nanosized state, is explained by a violation of the magnetic order in the subsurface layer of the particles. In this case, the magnetic moments of magnetically active atoms demonstrate the state of spin glasses [5, 6]. The size of such surface layers with noncollinear spins calculated as a result of measuring the dependence of the specific saturation magnetization on the specific surface area of the powders is 1–2 nm [7]. It is this layer, called the magnetic dead layer, that causes a decrease in magnetization. The magnetization decreases, as compared with the magnetization of the bulk material, because a large number of atoms constituting nanoparticles are located in the subsurface layer. Moreover, as a result of the propagation of the inactive magnetic layer to the whole particle following a decrease in its size, the particle acquires superparamagnetic properties [8]. The magnetic moment of such particles can change its direction randomly depending on the temperature. When there is no external magnetic field, the mean magnetization of superparamagnetic particles equals zero. A decrease in the magnetization obviously affects the consumer performance of the material [9, 10]. Thus, at the moment, superparamagnetism observed in nanoparticles above the blocking temperature is one of the main obstacles for the creation of high-density magnetic memory devices [11, 12].

In our study, we synthesised $Co_{0.65}Zn_{0.35}Fe_2O_4$ ferrite powders of various degrees of dispersion using the sol-gel method. We used a fixed ratio of the cobalt-zinc ferrite with a spinel structure because this composition has the highest specific saturation magnetization [13, 14]. The sol-gel method was used because it enabled us to control the microstructure of ferrite powders during the synthesis [15–18].

The purpose of our study was to develop control parameters for the sol-gel synthesis in order to identify effective methods for obtaining ferrite powders with increased magnetization, degree of crystallinity and the intermediate particles size between a superparamagnetic and a multidomain state. The material obtained as a result, can be used as a filler for coatings absorbing microwave radiation.

2. Experimental

To obtain a $Co_{0.65}Zn_{0.35}Fe_2O_4$ cobalt-zinc ferrite, a sol was formed by mixing a citric acid solution and a solution of metal nitrates. All the initial reagents were of analytical grade. The solution of metal nitrates was obtained by dissolving $Co(NO_3)_2 \cdot 6H_2O$, $Zn(NO_3)_2 \cdot 6H_2O$, $Fe(NO_3)_3 \cdot 9H_2O$ with a stoichiometric ratio of metal ions Co:Zn:Fe = 0.65:0.35:2.0 and the total concentration C(Me) = 0.3 mol/dm³ in distilled water. The aqueous solution of citric acid with the concentration $C(C_6H_8O_7)$ = 0.9 mol/dm³ was obtained by dissolving $C_6H_8O_7 \cdot H_2O$ in distilled water. The sol was formed by adding the citric acid solution to the solution of metal nitrates with vigorous stirring for 4 hours. By adding a 25% ammonia solution we obtained a neutral mixture with pH = 7. By heating at 90 °C the sol was transformed into a gel formed due to a significant increase in the volume concentration of the dispersed phase. As a result of the following thermal treatment (at 90 °C) we obtained a glass-shaped gel which was heated at 450 °C for 5 hours in order to remove any traces of carbon. The synthesised powder was washed with distilled water and dried in air. During the last stage, the powder was thermally treated at 500, 700, 900, and 1150 °C for 2 hours.

The samples were analysed using several physical and chemical methods.

X-ray diffraction patterns of the powder samples were registered using a DRON-2.0 diffractometer with CoK_α-radiation (λ = 0.178896 nm) and a Ni monochromator. Scanning was carried out in the range of angles 2θ = 20–80°.

The microstructure and the morphology of the nanoparticles were studied by means of scanning electron microscopy using a LEO 1455 VP microscope. For this, a thin layer of the powder suspension was deposited on sitall plates. Simultaneously the ratio of the concentration of metal atoms in ferrite powders and the features of their distribution on the surface of the particles were determined by energy dispersive X-ray spectroscopy (EDX-analysis).

The specific saturation magnetization and the coercive force were studied using the Cryogen Free Measurement System by Cryogenic Ltd.

The sizes of coherent scattering regions (CSR) corresponding to the size of the crystallites of the obtained ferrite were determined by the broadening of diffraction reflections (Scherrer method).

The following expressions was used to perform calculations according to the Scherrer method:

$$\beta = \frac{K\lambda}{D\cos\theta} \Rightarrow \cos\theta = \frac{K\lambda}{D}\frac{1}{\beta}, \quad (1)$$

where β is the width of the reflection at half height, rad; D is the size of the CSR, nm; K is the dimensionless particle drag coefficient (the Scherrer constant), λ is the wavelength of X-ray radiation, nm; and θ is the diffraction angle, rad.

Coefficient K may vary depending on the shape of the particles. For spherical particles K is usually assumed to be 0.9, while for cubic crystals the Scherrer constant can be calculated for each reflection using the following formula:

$$K = \frac{6|h|^3}{\sqrt{h^2+k^2+l^2}\,(6h^2 - 2|hk| + |kl| - 2|hl|)}, \quad (2)$$

where h, k, and l are Miller indices.

Lattice parameter a for a cubic cell is determined using the ratio:

$$a = d\sqrt{h^2+k^2+l^2}, \quad (3)$$

where d is the interplanar distance.

The shortest distance between the magnetic ions in tetrahedral (A) and octahedral (B) nodes of the lattice, also called the jump distance, considering the lattice constant was calculated using the following ratios [19]:

$$L_A = \frac{a\sqrt{3}}{4}, \quad (4)$$

$$L_A = \frac{a\sqrt{2}}{4}. \quad (5)$$

The theoretical X-ray density can be determined based on the X-ray diffraction patterns using the ratio [19] and taking into account the fact that each unit cell in the spinel structure consists of eight formula units,

$$N = \sum \frac{8M}{N_A \cdot a^3}, \quad (6)$$

where M is the molecular weight of the ferrite, N_A is Avogadro number, and a^3 is the unit cell volume.

3. Results and discussion

Fig. 1 demonstrates X-ray diffraction patterns of $Co_{0.65}Zn_{0.35}Fe_2O_4$ powders annealed at various temperatures. The study determined that when the sol-gel method is used, the phase with a spinel structure forms directly after the synthesis without any additional thermal treatment. Iron-citrate complexes are formed at higher concentrations of citric acid (2:1), and their compositions depend significantly on the pH of the solution. In this case, citric acid is used as a chelating agent.

Diffraction peaks of the cubic spinel are indexed as crystallographic planes: (111), (220), (311), (222), (400), (422), (511), and (440), which corresponds to the face-centred cubic crystal structure (JCPDS 22-1086) with the space group *Fd-3m*. Intensive reflections of the sample annealed at 900 °C demonstrate that $Co_{0.65}Zn_{0.35}Fe_2O_4$ nanoparticles are well-crystallized at this temperature. The average size of the crystallites of the obtained dispersed powders calculated using the Scherrer equation is given in Table 1. The study demonstrated that at higher annealing temperatures the perfection of the structure, crystallinity, and the size of the particles improve. In this case, not only does the intensity of the characteristic X-ray reflections of the spinel grow, but their broadening decreases for the annealing temperature range of 200–500 °C. This also indicates an increase in the size of the crystallites, a decrease in the degree of their defectiveness, a decrease in the inhomogeneity of the composition, and an increase in the degree of crystallinity. For instance, the average size

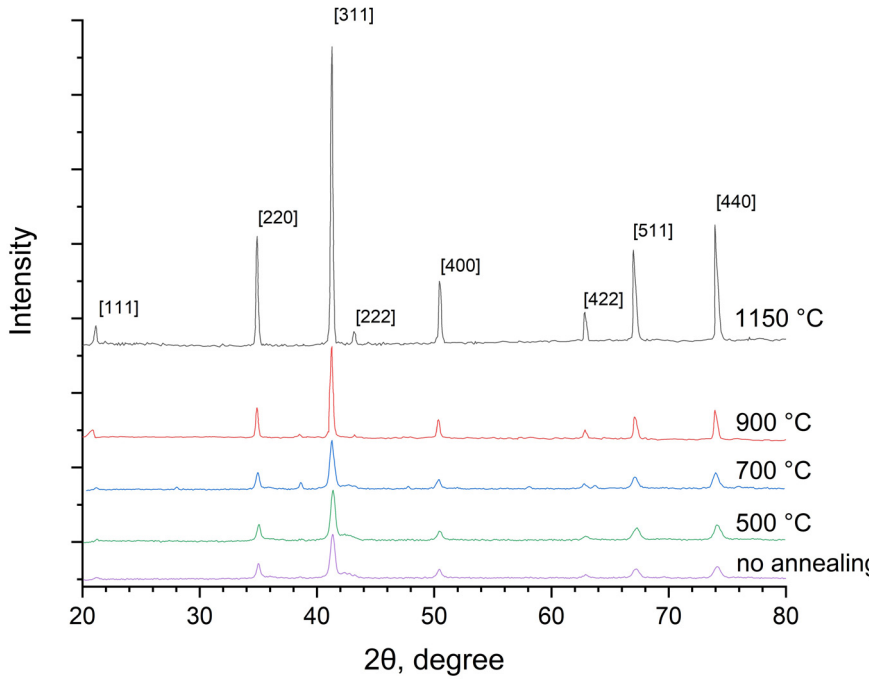

Fig. 1. X-ray diffraction patterns of the obtained powders

Table 1. Calculated and observed size of the crystallites

Annealing temperature, °C	Crystallite size by average peak, nm	Crystallite size by reflection (311), nm	Particle size (SEM), nm
0	20.8	20.6	–
500	20.6	21.0	40
700	23.5	21.3	80
900	63.8	59.4	150
1150	77.0	89.1	900

of crystallites for the CoZn ferrite obtained by the sol-gel method changed from 20 to 77 nm when annealed at 500 and 1150 °C. Some studies attribute such a growth of crystallites following an increase in the annealing temperature to the so-called Ostwald ripening effect [20, 21]. The analysis of the X-ray diffraction patterns demonstrated that when the temperature of annealing decreases after the synthesis, the background of the spectrum grows, and its reference line rises. This means that the particles are not fully crystallised and the fraction of the amorphous phase close to the crystal material increases. Obviously, this has a negative effect on the magnetic properties of the samples, for instance, on the specific saturation magnetization [22]. The study demonstrated that the lattice constants of these samples varied from 8.401 to 8.420 Å. They were calculated for the cubic phase of the spinel. The calculated jump distance and the length of the bond for tetrahedral (A) and octahedral (B) nodes of the lattices of the studied samples are given in Table 2. We should note that the X-ray density of the obtained samples tends to decrease. This can be explained by the redistribution of cations in the sublattices and changes in the degree of crystallinity.

Fig. 2 presents SEM images of the powders annealed at various temperatures. The images of the microstructure demonstrate that the powders annealed at low temperatures consist of dispersed aggregated and agglomerated particles of a nearly spherical shape. When the temperature of annealing increases, we observe the formation of larger particles which are slightly faceted and agglomerated. The agglomeration of particles can be caused by magneto-dipole interaction decreasing with an increase in the annealing temperature and the growth of the particles. After annealing at 900 °C, the images of the powders showed that the particles increased in size and acquired an ellipsoid shape. When the

Table 2. Calculation of the parameters of the crystal lattice

Annealing temperature, °C	Lattice constant *a*, Å	Jump length at tetrahedral lattice sites, Å	Jump length at octahedral lattice sites, Å	Radiographic density, g/cm³
0	8.401	3.64	2.97	5.30
500	8.401	3.64	2.97	5.30
700	8.412	3.64	2.97	5.29
900	8.416	3.64	2.98	5.28
1150	8.420	3.65	2.98	5.27

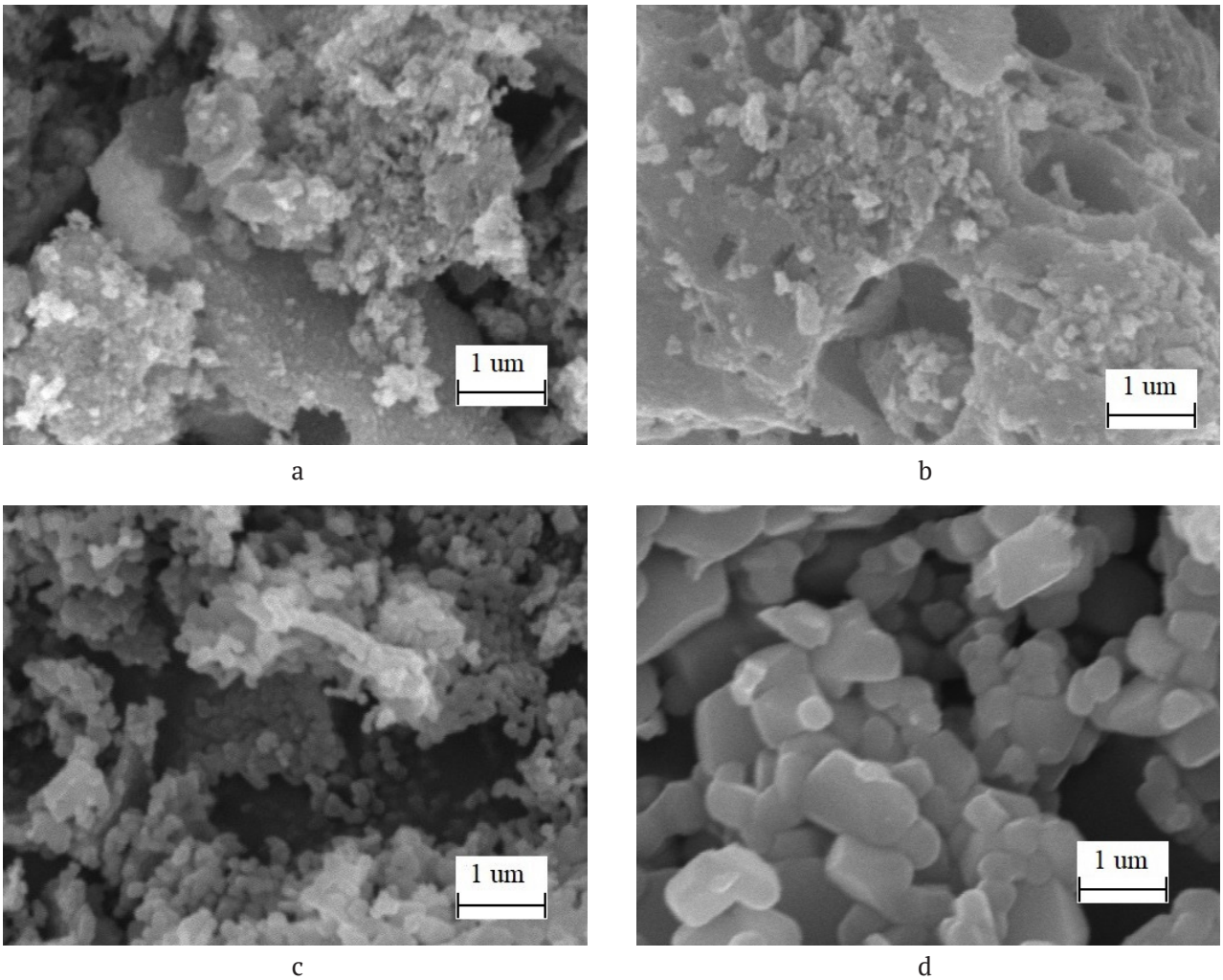

a b c d

Fig. 2. SEM images of CoZn ferrite powders annealed at 500 °C (a), 700 °C (b), 900 °C (c), and 1150 °C (d)

annealing temperature was further increased to 1150 °C, the particles grew rapidly to 1 μm. The start of the crystallisation of the samples with tetrahedral faceting was observed. The growth of the particles, presumably, proceeds according to the Ostwald ripening mechanism. [20, 21].

Since the average size of the crystallites is about 30 nm, the particles annealed at high temperatures include several separate crystallites. The number of crystallites in one particle decreases at lower annealing temperatures reaching 1. The samples annealed at lower temperatures have a morphology of irregular shape and are agglomerated.

To determine the ratio of metal ions in the synthesised CoZn ferrite, we performed energy

dispersive X-ray spectroscopy of the sample annealed at 700 °C. The analysis determined that the amount of iron, cobalt, zinc, and oxygen corresponds to the formula $Co_{0.64}Zn_{0.35}Fe_{2.01}O_4$, which is in agreement with the target composition.

To determine the magnetic properties of the powders, we analysed the field dependences of the specific magnetization in the magnetic field $H = \pm 4$ T. Magnetization curves presented in Fig. 3 indicate the presence of the magnetic order in the analysed samples. Based on the changes in the specific magnetization of the particles of the Co-Zn ferrite depending on the strength of the external magnetic field, we can conclude that the magnetization curves of the samples annealed at 900 and 1150 °C reach the saturation region, when the strength of the magnetic field is over 3 T. This could mean that the type of the magnetic order is close to the ferrimagnetic. The study determined that the slope of the obtained curves and the saturation magnetization increase significantly following the growth of the annealing temperature. This can be interpreted as an indication of a significant decrease in the size of the inactive magnetic layer on the surface of the nanoparticles. Besides the noncollinearity of spins, this layer can also have a composition different from that of the nucleus of the particle because the process of reciprocal diffusion of cations during the spinel synthesis is not complete. We can assume that disordering of cations and defectiveness can also take place in this layer. We should also remember the possibility that the formation of the spinel structure can be incomplete. This is indicated by broad reflections of the spinel phase on the X-ray diffraction patterns, which indicates the existence of different compositions of the material with different lattice constants. The existence of an amorphous material in this layer during certain synthesis stages is also possible.

Despite the fact that an increase in the annealing temperature (as determined for the sol-gel method) results in the growth of the specific magnetization of the CoZn ferrites, it does not reach the values characteristic for bulk samples, yet alone for single crystals (~98 $A \cdot m^2 \cdot kg^{-1}$) for $Co_{0.65}Zn_{0.35}Fe_2O_4$ [23]. This is also explained by the existence of the inactive magnetic layer on the surface of the nanoparticles, since a decrease in its fraction following an increase in the annealing temperature and a decrease in the surface area of the nanopowders during thermal treatment results in a significant increase in the saturation magnetization of the highly dispersed material.

As demonstrated by the study, a decrease in the size of the nanoparticles to several nanometres results in their transition to the

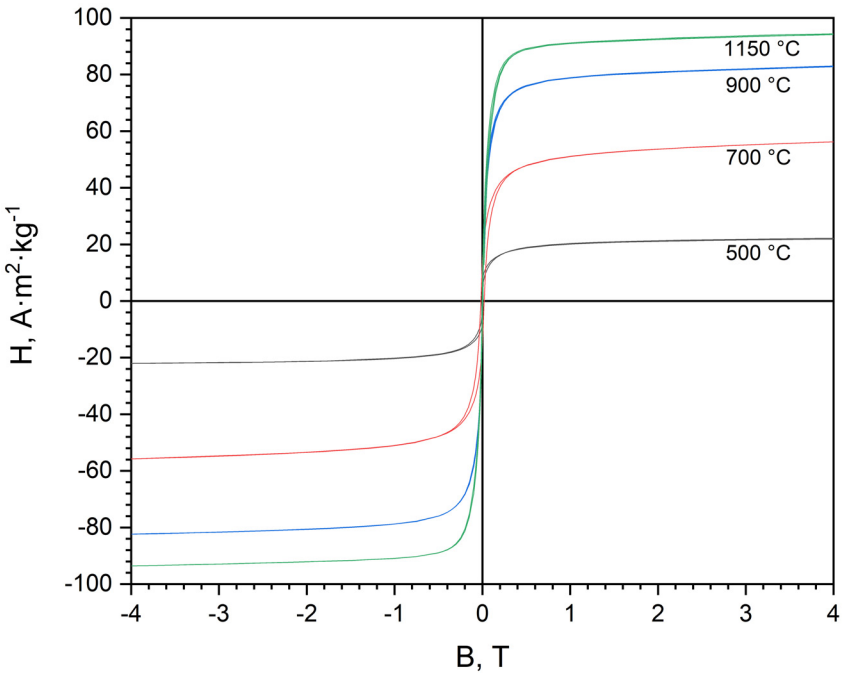

Fig. 3. Magnetization curves for the annealed CoZn ferrite powders

superparamagnetic state due to the propagation of the magnetic dead layer over the whole particle. According to the literature data, the critical size of the cobalt ferrite nanoparticles for the transition to the superparamagnetic state lies within the range of up to 10 nm [24]. There is also a critical size value below which the particles become single-domain. If a ferrimagnetic particle has a domain structure, i.e. is multidomain, its remagnetization proceeds due to the displacement of the domain borders. In this case, the coercive force is low and grows with a decrease in the size of the particles. The coercive force is at maximum when the particles are single-domain. An increase in H_C during the transition to the single-domain structure is connected with a different remagnetization mechanism, namely the transition from the displacement of the borders to the coherent rotation of the magnetic order of the particle [25]. In our study, the coercive force of the powders annealed at 900 °C was 2.228 kA·m^{-1} and for the powders annealed at 1150 °C it was 3.167 kA·m^{-1}.

During the further decrease in the size of the nanoparticles following a transition from the multidomain to the single-domain state, superparamagnetism is observed. Thus, for the cobalt ferrite the critical size for the transition of the particles to the single-domain state is slightly below 50 nm [26]. Therefore, when the diameter of the particles decreases in the range from 50 to 10 nm the degree of superparamagnetism for cobalt ferrite nanopowders increases. In other words, we observe the so-called blocking process [27]. The main reason why the single-domain state has the greatest energetic advantage is the fact that with a decrease in the size of the particles, the fraction of the surface energy on the domain borders increases and becomes larger that the bulk energy of the sample. [25]. When the size of the particles in the single-domain state decreases, H_C decreases. This phenomenon is explained by the influence of thermal fluctuations on the magnetic anisotropy value, which in turn is connected with the coercive force. Superparamagnetism occurs in the surface layer of the nanoparticle when the energy barrier of the magnetic anisotropy is overcome due to the thermal activation, which results in fluctuations of the magnetization in the surface layer [28]. The residual magnetization Mr and H_C in the superparamagnetic state is zero [29].

The study demonstrated that for the cobalt-zinc ferrite obtained by means of the sol-gel method the annealing following the synthesis changes the size of the crystallites from 20 to 77 nm. At the same time the size of the particles changes from 40 to 950 nm. Taking into account the fact that the critical value for the transition to the single-domain state is 50 nm, the analysed particles of the cobalt-zinc ferrite with the size smaller than 50 nm have a certain degree of seperparamagnetism. This is true for the annealing temperatures below 700 °C.

As we mentioned before, the highest values of the coercive force correspond to the transition boundary between the multidomain and single-domain particles. With a decrease in the size, the coercive force decreases in the superparamagnetic area or in the blocking area. It is zero for superparamagnetic particles. In the latter case, the hysteresis disappears. Thus, for the annealing temperatures of 500 and 700 °C the coercive force of the studied powders was 2.992 kA·m^{-1} and 15.199 kA·m^{-1} respectively.

For lower annealing temperatures and small sizes of the crystallites we observed prominent superparamagnetic behaviour of the samples at room temperature. This indicates the presence of an abnormally large coercive force for the powder annealed at 700 °C (Table 3). This can be explained by the fact that the obtained materials are on the border between multidomain and single-domain states, when the coercive force reaches its maximum. For higher annealing temperatures, when the particles are larger, the hysteresis curves demonstrate a prominent coercive force, which indicates the presence of only an insignificant degree of superparamagnetism.

Table 3. Magnetic properties of the obtained powders

Annealing temperature, °C	Saturation magnetization, A·m^2·kg^{-1}	Coercive force, kA·m^{-1}
500	21.8	2.992
700	56.1	15.199
900	83.0	2.228
1150	94.1	3.167

In this case, only a small number of particles of the size smaller than critical transit to the superparamagnetic state. This is important for obtaining the materials sensitive to microwave radiation.

For the obtained powders of the Co-Zn ferrite the specific magnetization in the 4 T field for the annealing temperatures of 900 and 1150 °C was above 80 $A \cdot m^2 \cdot kg^{-1}$. The size of the particles was 150 and 950 nm respectively. A different situation was observed, when the size of the particles was significantly smaller and therefore they had a larger surface-volume ratio. In this case, several effects including the broken bonds between the atoms on the surface resulting in the random spin orientation reduce the coordination of the surface atoms and result in a decrease in the magnetiszation due to an increase in the surface anisotropy. Thus, the study demonstrated that for the particles of the Co-Zn ferrite of an average size of 40 nm the specific saturation magnetisation is 21.8 $A \cdot m^2 \cdot kg^{-1}$, and for the 80 nm particles the specific saturation magnetisation is 56.1 $A \cdot m^2 \cdot kg^{-1}$.

4. Conclusions

The study determined that for highly dispersed particles with a changed magnetic order and crystal structure on the surface, an inactive magnetic layer is formed. The size of the layer can reach up to 50 % of the volume of the particles. [30]. This has a negative effect on the magnetisation of the nanoparticles. Taking into account the above described facts, when developing dispersed particles which could be used as fillers for the devices interacting with microwave radiation, it is advisable to maintain the balance between high magnetic characteristics and the acceptable degree of dispersion of the particles. From the point of view of sol-gel synthesis, the obtained dependences of magnetic properties and the degree of dispersion on the thermal treatment temperature of the synthesised powders can be used to determine optimal conditions. Based on this dependence we suggested a material for absorption of microwave radiation based on the dispersed powder of the CoZn ferrite annealed at 900 °C after the sol-gel synthesis.

Contribution of the authors

The authors contributed equally to this article.

Conflict of interests

The authors declare that they have no known competing financial interests or personal relationships that could have influenced the work reported in this paper.

References

1. Houbi A., Aldashevich Z. A., Atassi Y., Telmanovna Z. B., Saule M., Kubanych K. Microwave absorbing properties of ferrites and their composites: A review. *Journal of Magnetism and Magnetic Materials*. 2021;529: 167839. https://doi.org/10.1016/j.jmmm.2021.167839

2. Yin P., Zhang L., Feng X., Wang J., Dai J., Tang Y. Recent progress in ferrite microwave absorbing composites. *Integrated Ferroelectrics*. 2020;211(1): 82–101. https://doi.org/10.1080/10584587.2020.1803677

3. Kodama R. H., Berkowitz A. E., McNiff Jr E. J., Foner S. Surface spin disorder in ferrite nanoparticles. *Journal of Applied Physics*. 1997;81(8): 5552–5557. https://doi.org/10.1063/1.364659

4. Thakur P., Taneja S., Chahar D., Ravelo B., Thakur A. Recent advances on synthesis, characterization and high frequency applications of Ni-Zn ferrite nanoparticles. *Journal of Magnetism and Magnetic Materials*. 2021;530: 167925. https://doi.org/10.1016/j.jmmm.2021.167925

5. Martinez B., Obradors X., Balcells L., Rouanet A., Monty C.. Low temperature surface spin-glass transition in γ-Fe_2O_3 nanoparticles. *Physical Review Letters*. 1998;80(1): 181. https://doi.org/10.1103/PhysRevLett.80.181

6. Leite E. S., Coaquira J. A., Viali W. R., Sartoratto P. P., De Almeida R. L., Morais P. C., Malik S. K. Spin-glass-like characteristics of extremely small γ-Fe_2O_3 nanoparticles. Journal of Physics: Conference Series. 2010;200(7): 072060. https://doi.org/10.1088/1742-6596/200/7/072060

7. El-Sayed H. M., Ali I. A., Azzam A., Sattar A. A. Influence of the magnetic dead layer thickness of Mg-Zn ferrites nanoparticle on their magnetic properties. *Journal of Magnetism and Magnetic Materials*. 2017;424: 226–232. https://doi.org/10.1016/j.jmmm.2016.10.049

8. Khah F. M., Arab A., Kiani E. The effect of thickness of the dead layer on the magnetization of $Ni_{0.5-x}Co_xZn_{0.5}Fe_2O_4$ ferrite nanopowders and determination of optimal permeability. *Journal of Superconductivity and Novel Magnetism*. 2021;34: 2699–708. https://doi.org/10.1007/s10948-021-05976-x

9. Singh J. P., Dixit G., Srivastava R. C., Agrawal H. M., Reddy V. R., Gupta A. Observation of bulk like magnetic ordering below the blocking temperature in

nanosized zinc ferrite. *Journal of magnetism and magnetic materials*. 2012;324(16): 2553–2559. https://doi.org/10.1016/j.jmmm.2012.03.045

10. Meidanchi A., Ansari H. Copper spinel ferrite superparamagnetic nanoparticles as a novel radiotherapy enhancer effect in cancer treatment. *Journal of Cluster Science*. 2021;32: 657–663. https://doi.org/10.1007/s10876-020-01832-5

11. Sharma R., Thakur P., Sharma P., Sharma V. Ferrimagnetic Ni^{2+} doped Mg-Zn spinel ferrite nanoparticles for high density information storage. *Journal of Alloys and Compounds*. 2017;704: 7–17. https://doi.org/10.1016/j.jallcom.2017.02.021

12. Harasawa T., Suzuki R., Shimizu O., Olcer S., Eleftheriou E. Barium-ferrite particulate media for high-recording-density tape storage systems. *IEEE transactions on magnetics*. 2010;46(6): 1894–1897. https://doi.org/10.1109/TMAG.2010.2042286

13. Nasrin S., Hoque S. M., Chowdhury F. U., Hossen M. M. Influence of Zn substitution on the structural and magnetic properties of $Co_{1-x}Zn_xFe_2O_4$ nano-ferrites. *IOSR Journal of Applied Physics*. 2014;6(2): 58–65. https://doi.org/10.9790/4861-06235865

14. Vinosha P. A., Manikandan A., Ceicilia A. S., Dinesh A., Nirmala G. F., Preetha A. C., Slimani Y., Almessiere M. A., Baykal A., Xavier B. Review on recent advances of zinc substituted cobalt ferrite nanoparticles: Synthesis characterization and diverse applications. *Ceramics International*. 2021;47(8): 10512–10535. https://doi.org/10.1016/j.ceramint.2020.12.289

15. Kaur P., Chawla S. K., Meena S. S., Yusuf S. M., Pubby K., Narang S. B. Modulation of physico-chemical, magnetic, microwave and electromagnetic properties of nanocrystalline strontium hexaferrite by Co-Zr doping synthesized using citrate precursor sol-gel method. *Ceramics International*. 2017;43(1): 590–598. https://doi.org/10.1016/j.ceramint.2016.09.199

16. Sajjia M., Oubaha M., Hasanuzzaman M., Olabi A. G. Developments of cobalt ferrite nanoparticles prepared by the sol–gel process. *Ceramics International*. 2014;40(1): 1147–1154. https://doi.org/10.1016/j.ceramint.2013.06.116

17. Sutka A., Mezinskis G. Sol-gel auto-combustion synthesis of spinel-type ferrite nanomaterials. *Frontiers of Materials Science*. 2012;6(2): 128–141. https://doi.org/10.1007/s11706-012-0167-3

18. Ashour A. H., El-Batal A. I., Maksoud M. A., El-Sayyad G. S., Labib S. H., Abdeltwab E., El-Okr M. M. Antimicrobial activity of metal-substituted cobalt ferrite nanoparticles synthesized by sol–gel technique. *Particuology*. 2018;40: 141–151. https://doi.org/10.1016/j.partic.2017.12.001

19. Karimi Z., Mohammadifar Y., Shokrollahi H., Asl S. K., Yousefi G., Karimi L. Magnetic and structural properties of nano sized Dy-doped cobalt ferrite synthesized by co-precipitation. *Journal of Magnetism and Magnetic Materials*. 2014;361: 150–156. https://doi.org/10.1016/j.jmmm.2014.01.016

20. Shahbahrami B., Rabiee S. M., Shidpour R., Salimi-Kenari H. Influence of calcination parameters on the microstructure, magnetic and hyperthermia properties of Zn-Co ferrite nanoparticles. *Journal of Electroceramics*. 2022;48: 157–168. https://doi.org/10.1007/s10832-022-00281-y

21. Sakurai S., Nishino H, Futaba DN, Yasuda S, Yamada T, Maigne A, Matsuo Y, Nakamura E, Yumura M., Hata K. Role of subsurface diffusion and Ostwald ripening in catalyst formation for single-walled carbon nanotube forest growth. *Journal of the American Chemical Society*. 2012;134(4): 2148–2153. https://doi.org/10.1021/ja208706c

22. Rafeeq S. N., Ismail M. M., Sulaiman J. M. Magnetic and dielectric properties of $CoFe_2O_4$ and $Co_xZn_{1-x}Fe_2O_4$ nanoparticles synthesized using sol-gel method. *Journal of Magnetics*. 2017;22(3): 406–413. https://doi.org/10.4283/JMAG.2017.22.3.406

23. *Tables of physical quantities**. I. K. Kikoin (ed.). Moscow: Atomizdat Publ.; 1976. 1006 p. (In Russ.)

24. Karaagac O., Yildiz B. B., Köçkar H. The influence of synthesis parameters on one-step synthesized superparamagnetic cobalt ferrite nanoparticles with high saturation magnetization. *Journal of Magnetism and Magnetic Materials*. 2019;473: 262–267. https://doi.org/10.1016/j.jmmm.2018.10.063

25. Frolov G. I., Bachina O. I., Zav'yalova M. M., Ravochkin S. I. Magnetic properties of nanoparticles of 3*d* metals. *Technical Physics*. 2008;53(8): 1059–1064. https://doi.org/10.1134/s1063784208080136

26. Chinnasamy C. N., Jeyadevan B., Shinoda K., Tohji K., Djayaprawira D. J., Takahashi M., Joseyphus R. J., Narayanasamy A. Unusually high coercivity and critical single-domain size of nearly monodispersed $CoFe_2O_4$ nanoparticles. *Applied Physics Letters*. 2003;83(14): 2862–2864. https://doi.org/10.1063/1.1616655

27. Rao K. S., Nayakulu S. R., Varma M. C., Choudary G. S., Rao K. H. Controlled phase evolution and the occurrence of single domain $CoFe_2O_4$ nanoparticles synthesized by PVA assisted sol-gel method. *Journal of Magnetism and Magnetic Materials*. 2018;451: 602–608. https://doi.org/10.1016/j.jmmm.2017.11.069

28. Khader S. A., Sankarappa T. Dielectric, magnetic and ferroelectric studies in (x)$Mn_{0.5}Zn_{0.5}Fe_2O_4$ + (1–x) $BaTiO_3$ magnetoelectric nano-composites. *Materials Today*: *Proceedings*. 2016;3(6): 2358–2365. https://doi.org/10.1016/j.matpr.2016.04.148

29. Saffari F., Kameli P., Rahimi M., Ahmadvand H., Salamati H. Effects of Co-substitution on the structural and magnetic properties of $NiCo_xFe_{2-x}O_4$ ferrite nanoparticles. *Ceramics International*. 2015;41(6):

7352–7358. https://doi.org/10.1016/j.ceramint.2015.02.038

30. Negi D. S., Sharona H., Bhat U., Palchoudhury S., Gupta A., Datta R. Surface spin canting in Fe_3O_4 and $CoFe_2O_4$ nanoparticles probed by high-resolution electron energy loss spectroscopy. *Physical Review B*. 201730;95(17): 174444. https://doi.org/10.1103/PhysRevB.95.174444

** Translated by author of the article.*

Information about the authors

Dmitry V. Ivashenko, M. S. (Chemistry), Belarusian State University (Minsk, Belarus).
https://orcid.org/0000-0002-9149-7213
ivashenkodm@gmail.com

Diana A. Urbanovich, Belarusian State University (Minsk, Belarus).
https://orcid.org/0000-0002-5452-0277
urbanovichd00@gmail.com

Ilya Y. Palyn, Belarusian State University (Minsk, Belarus).
https://orcid.org/0000-0002-1542-8427
iliapolyn@gmail.com

Maxim V. Bushinsky, Cand. Sci. (Phys.–Math.), Head of the Laboratory of Non-metallic Ferromagnets SSPA "Scientific-Practical Materials Research Centre of National Academy of Sciences of Belarus" (Minsk, Belarus).
https://orcid.org/0000-0002-7234-6866
bushinsky@physics.by

Alexey V. Trukhanov, Dr. Sci. (Phys.–Math.), Deputy General Director for Research and Innovation SSPA "Scientific-Practical Materials Research Centre of National Academy of Sciences of Belarus" (Minsk, Belarus).
https://orcid.org/0000-0002-4387-8214
truhanov86@mail.ru

Vladimir V. Pankov, Dr. Sci. (Chem.), Professor at Department of Physical Chemistry, Belarusian State University (Minsk, Belarus). https://orcid.org/0000-0001-5478-0194
pankov@bsu.by

Received 11.10.2022; approved after reviewing 08.11.2022; accepted for publication 15.11.2022; published online 25.03.2023.

Translated by Yulia Dymant
Edited and proofread by Simon Cox